Supplementary Materials

What is the Trade-Off between Snowpack Stratification and Simulated Snow Water Equivalent in a Physically-Based Snow Model?

Julien Augas [1,*], Kian Abbasnezhadi [1,2], Alain N. Rousseau [1] and Michel Baraer [3]

[1] Institut National de la Recherche Scientifique, Centre Eau Terre Environnement (INRS-ETE), 490, Rue de la Couronne, G1K 9A9 Québec, QC, Canada; kian.abbasnezhadi@canada.ca (K.A.); Alain.Rousseau@ete.inrs.ca (A.N.R.)

[2] Climate Research Division, Science and Technology Branch, Environment and Climate Change Canada, 4905 Dufferin Street, M3H 5T4 Toronto, ON, Canada

[3] Hydrology, Climate and Climate Change Laboratory, École de technologie supérieure, University of Quebec, 1100 Notre-Dame Street West, H3C 1K3 Montreal, QC, Canada; michel.baraer@etsmtl.ca

* Correspondence: julien.augas@ete.inrs.ca

List of Figures

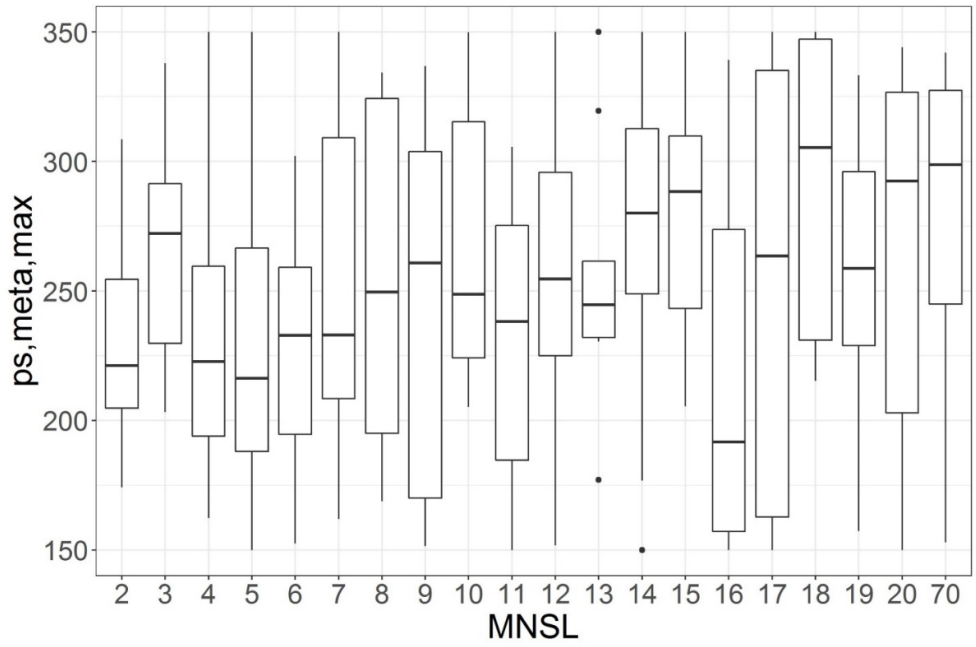

Figure S1. Snow layer density triggering the metamorphism phenomenon of the snow layer against the MNSL at GMON LF station.

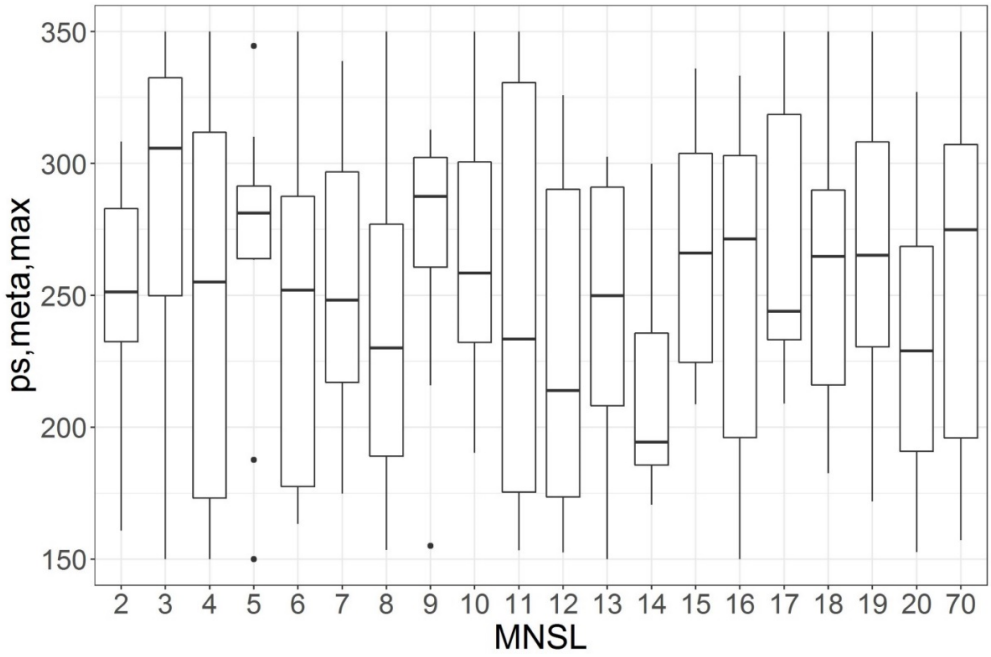

Figure S2. Snow layer density triggering the metamorphism phenomenon of the snow layer against the MNSL at GMON LL station.

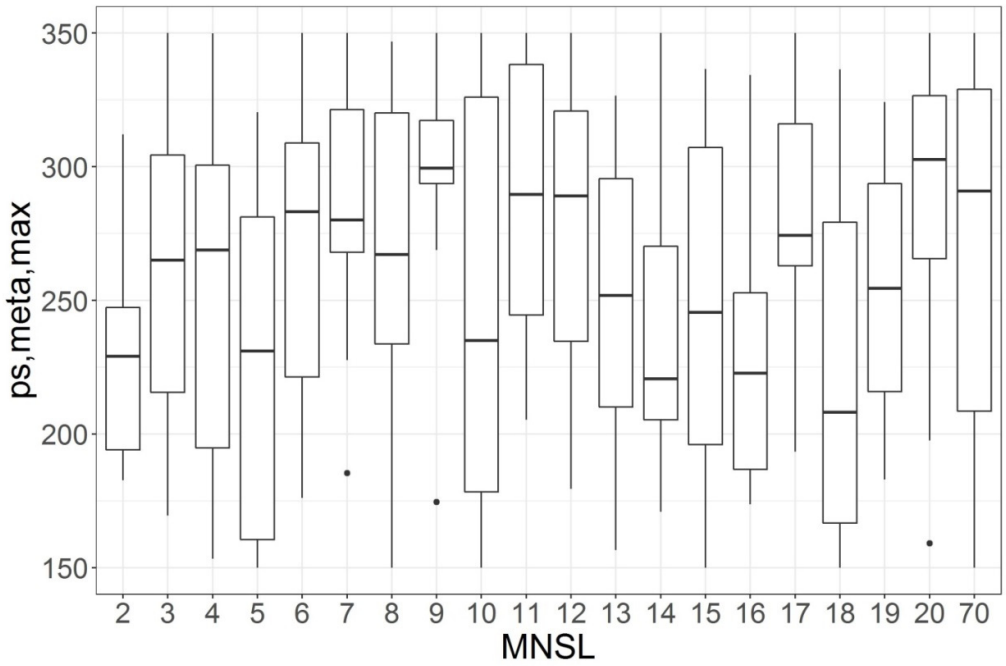

Figure S3. Snow layer density triggering the metamorphism phenomenon of the snow layer against the MNSL at GMON W station.

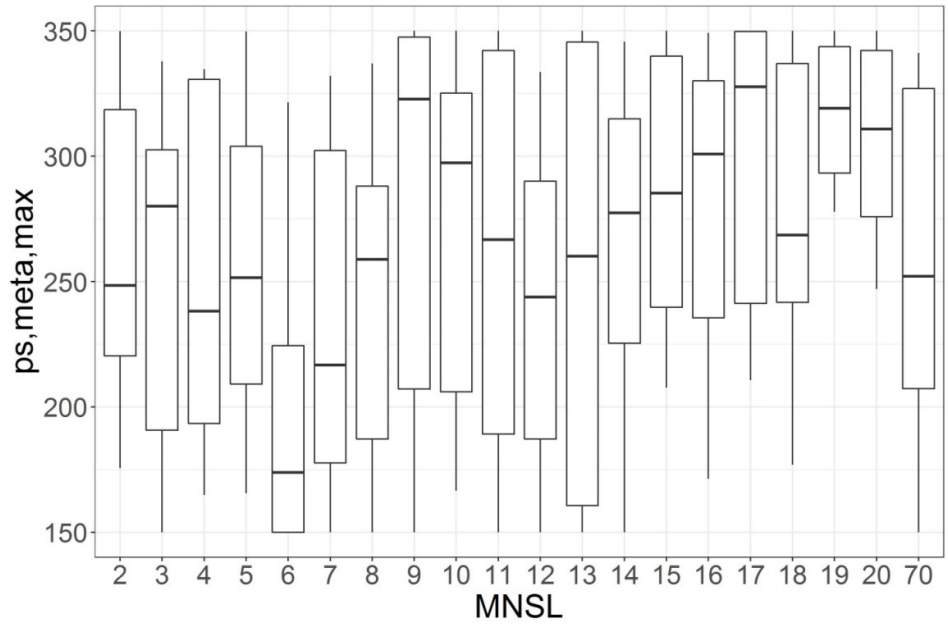

Figure S4. Snow layer density triggering the metamorphism phenomenon of the snow layer against the MNSL at GMON Neco station.

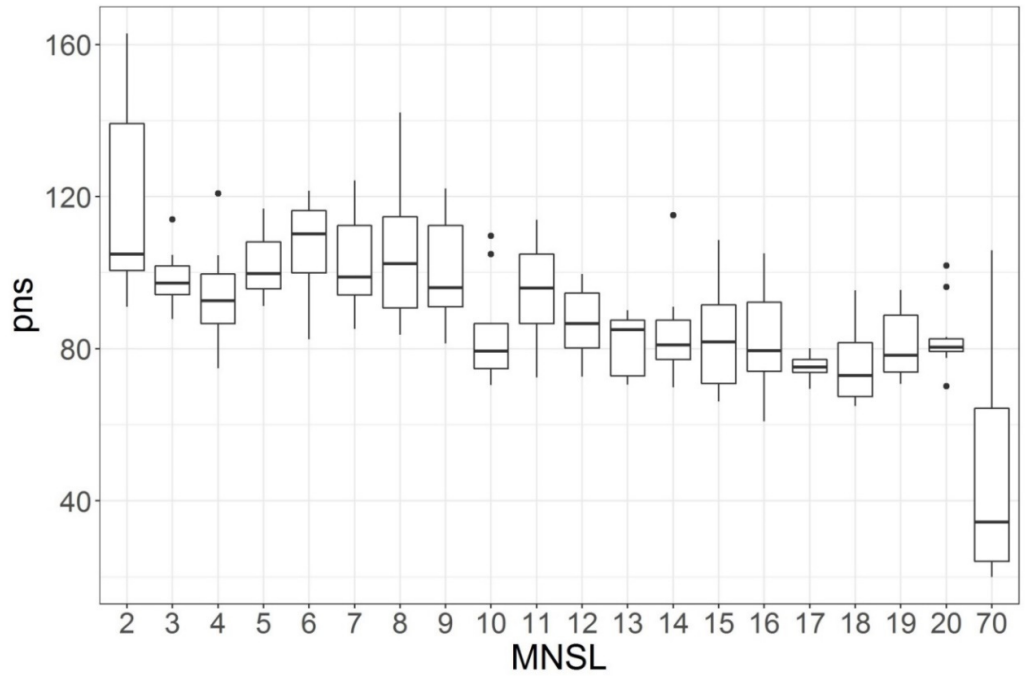

Figure S5. Fresh snow minimum density against the MNSL at GMON LF station.

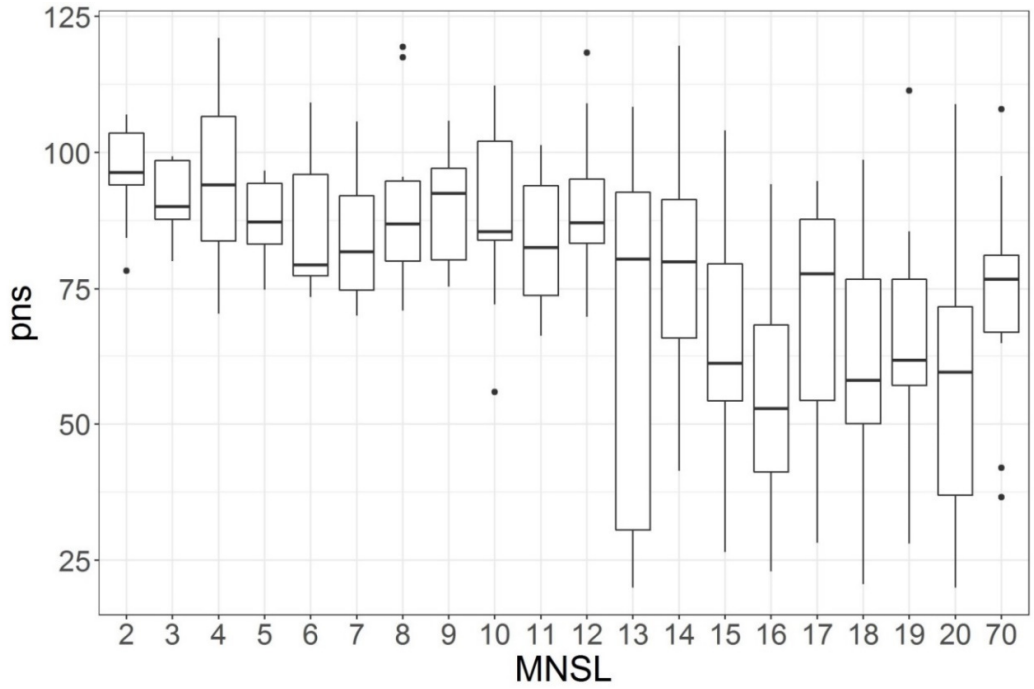

Figure S6. Fresh snow minimum density against the MNSL at GMON LL station.

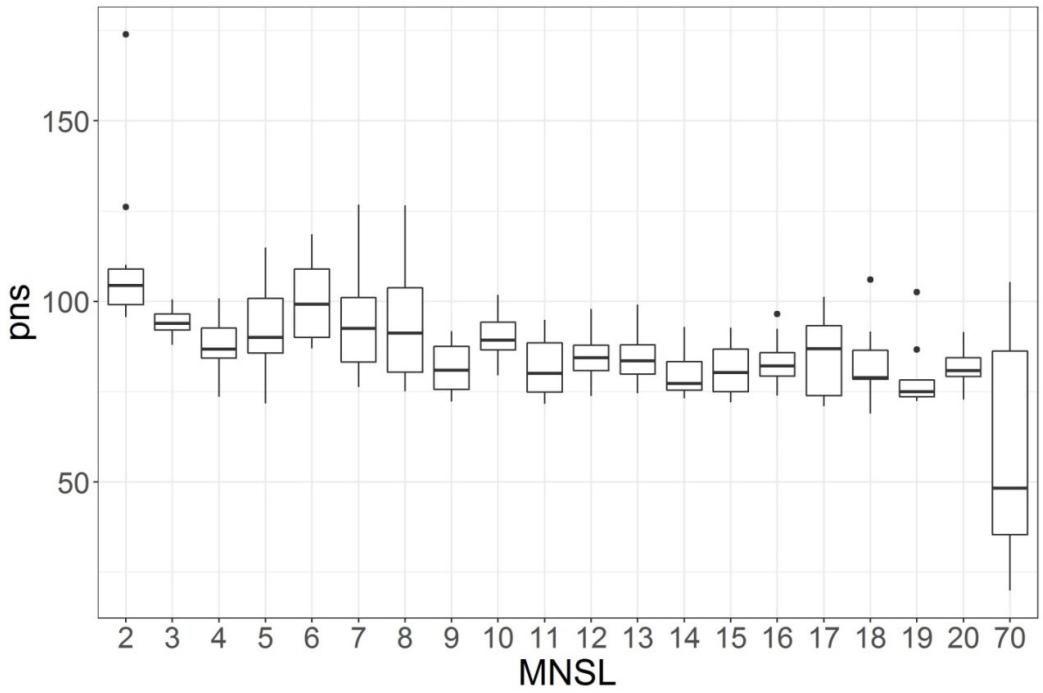

Figure S7. Fresh snow minimum density against the MNSL at GMON W station.

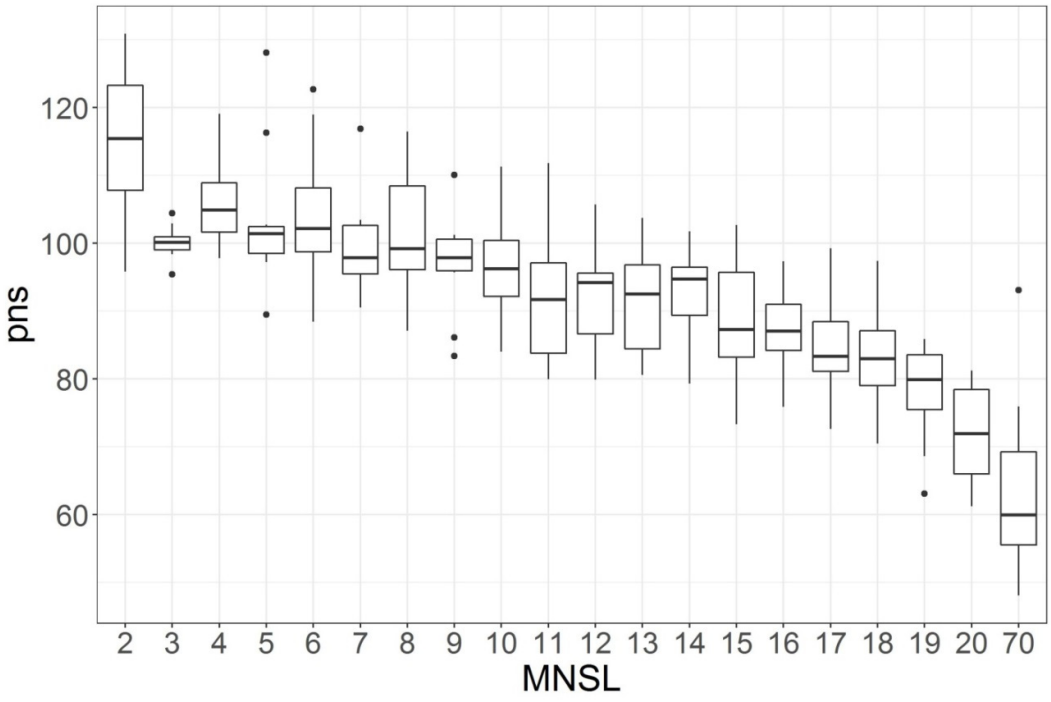

Figure S8. Fresh snow minimum density against the MNSL at GMON Neco station.

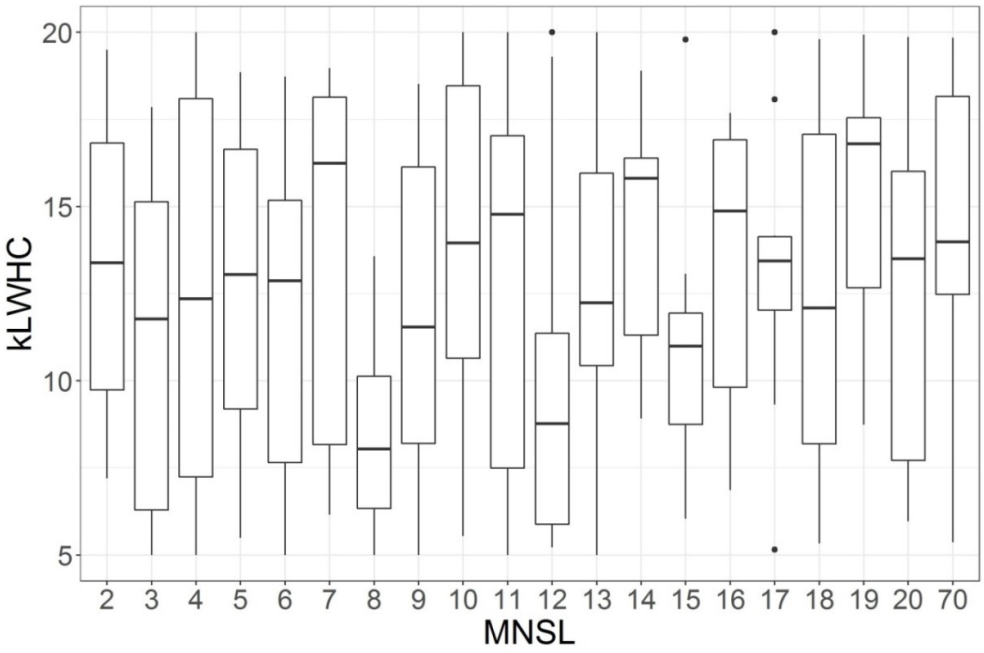

Figure S9. Maximum retention capacity of the snow layer against the MNSL at GMON LF station.

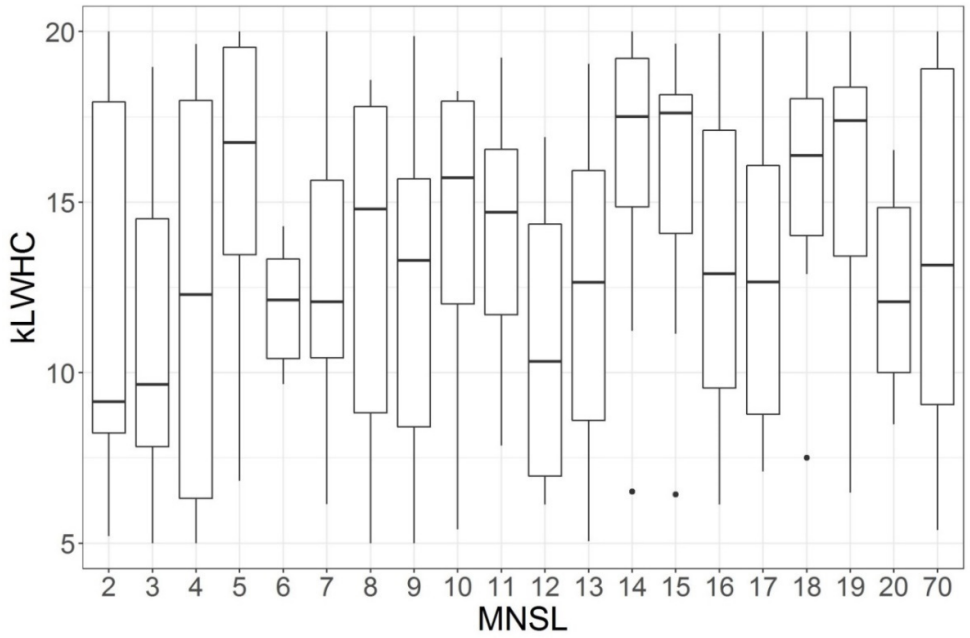

Figure S10. Maximum retention capacity of the snow layer against the MNSL at GMON LL station.

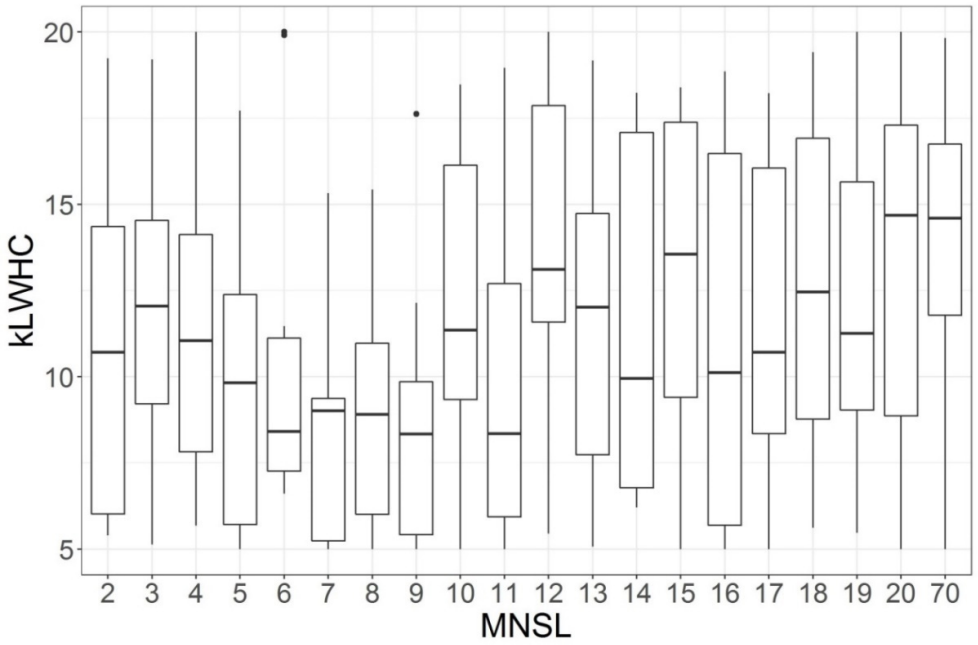

Figure S11. Maximum retention capacity of the snow layer against the MNSL at GMON W station.

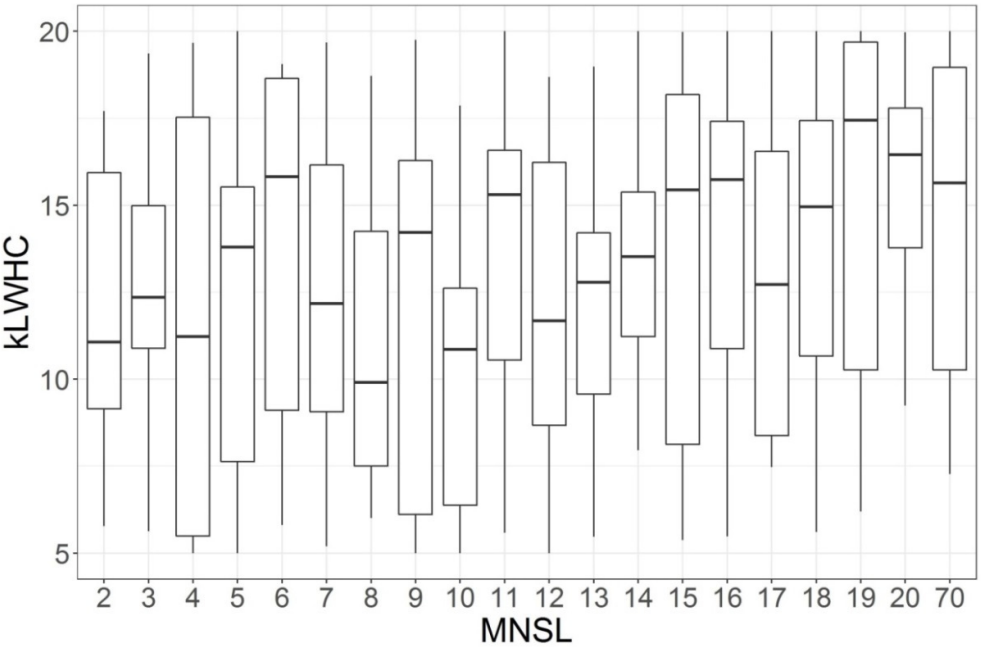

Figure S12. Maximum retention capacity of the snow layer against the MNSL at GMON Neco station.

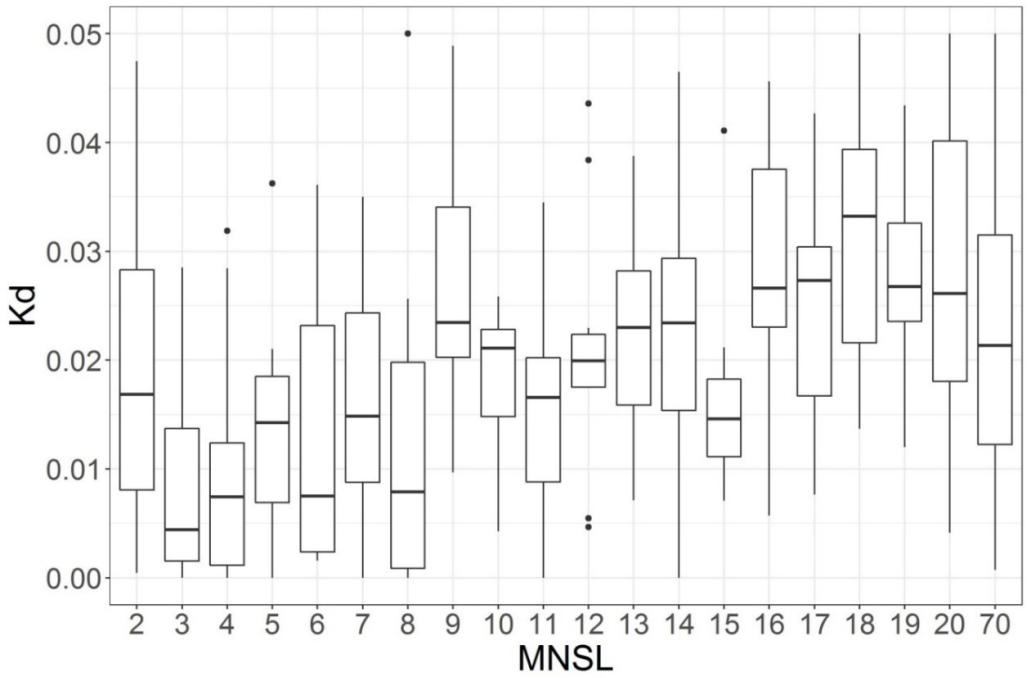

Figure S13. Settlement coefficient against the MNSL at GMON LF station.

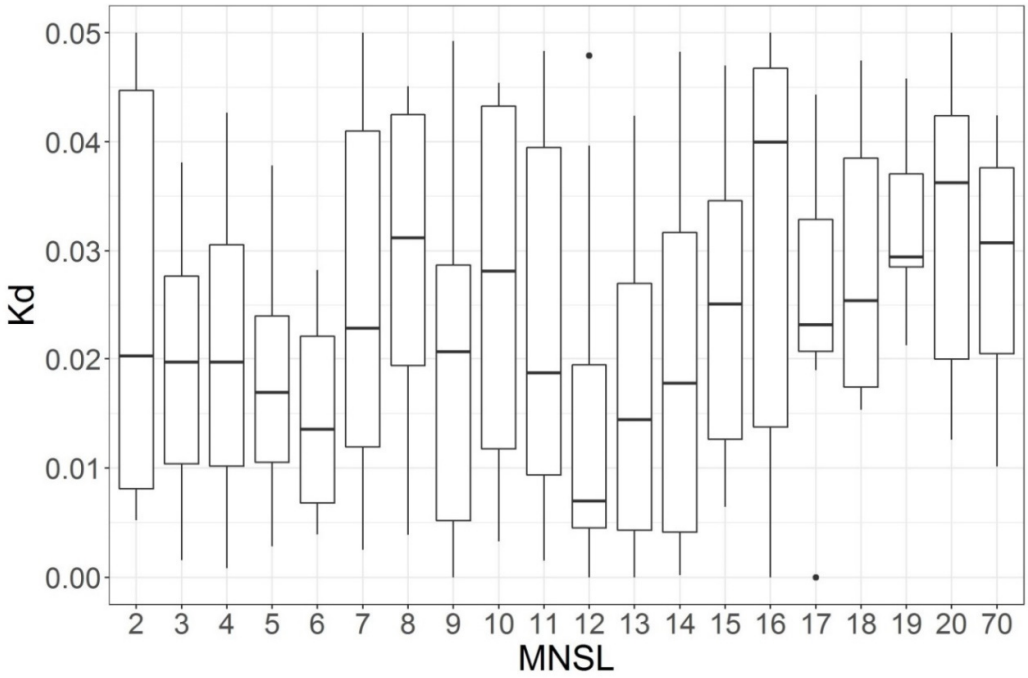

Figure S14. Settlement coefficient against the MNSL at GMON LL station.

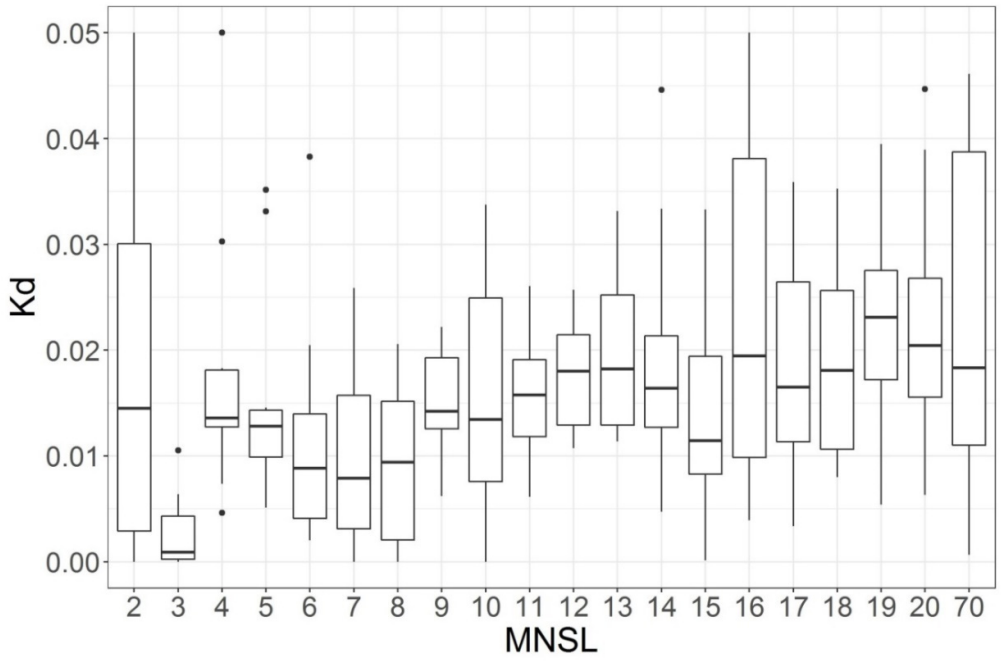

Figure S15. Settlement coefficient against the MNSL at GMON W station.

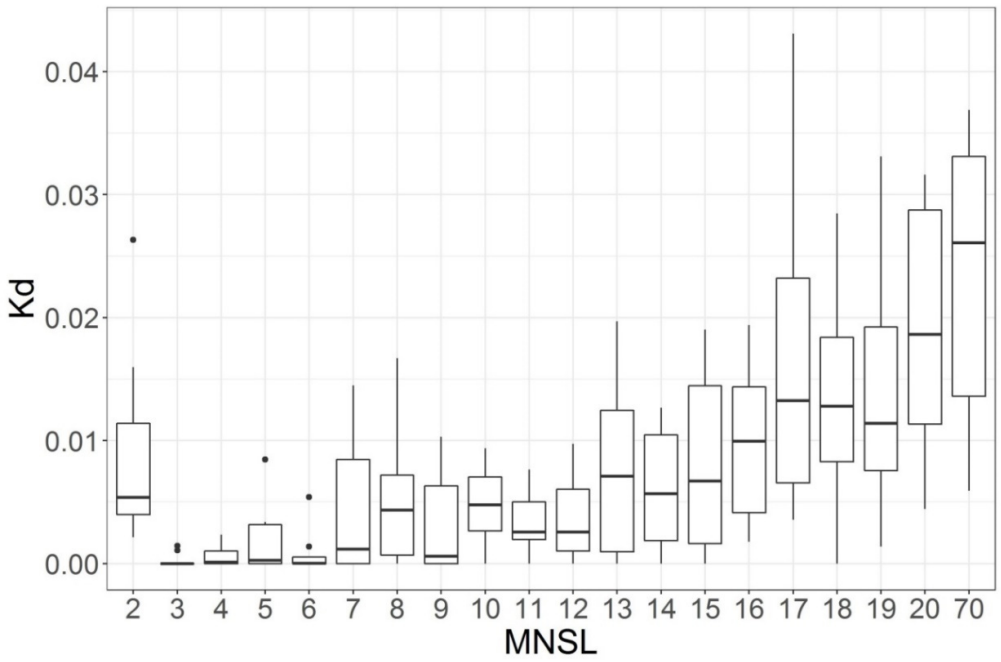

Figure S16. Settlement coefficient against the MNSL at GMON Neco station.

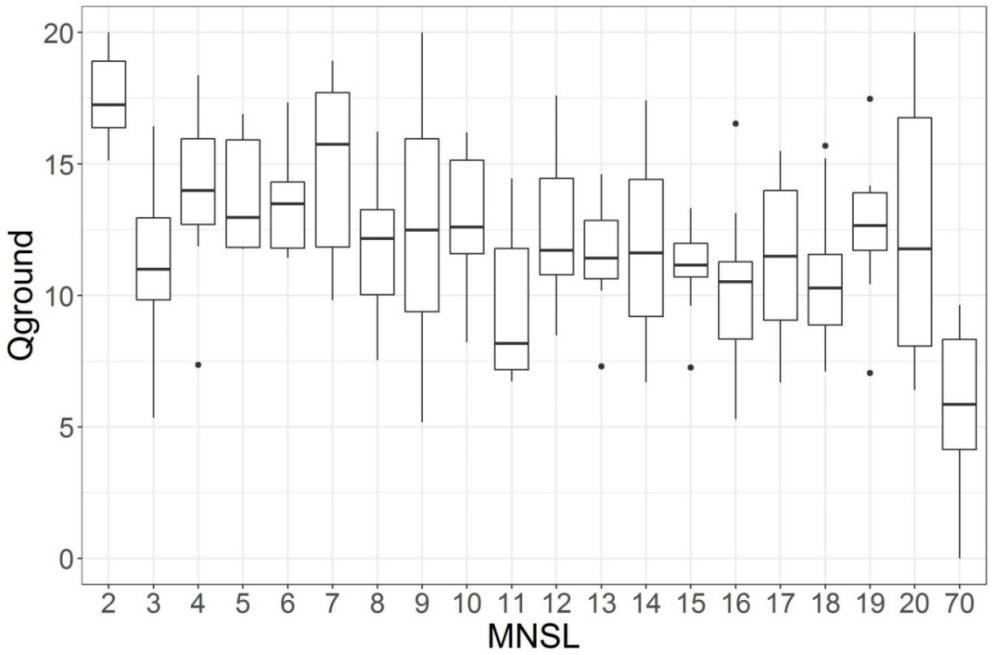

Figure S17. Ground heat flux against the MNSL at GMON LF station.

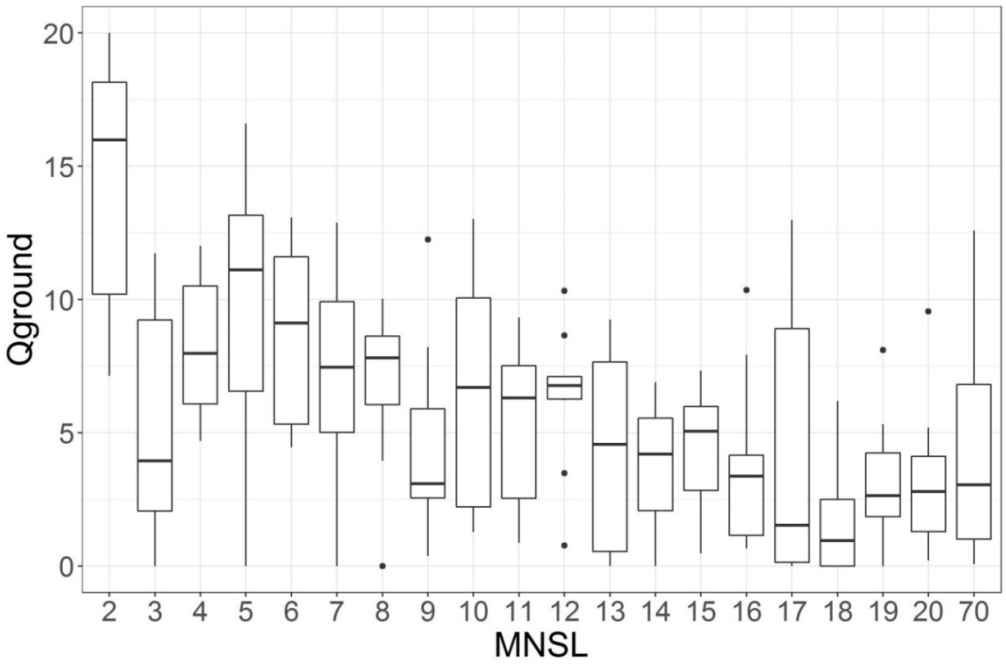

Figure S18. Ground heat flux against the MNSL at GMON LL station.

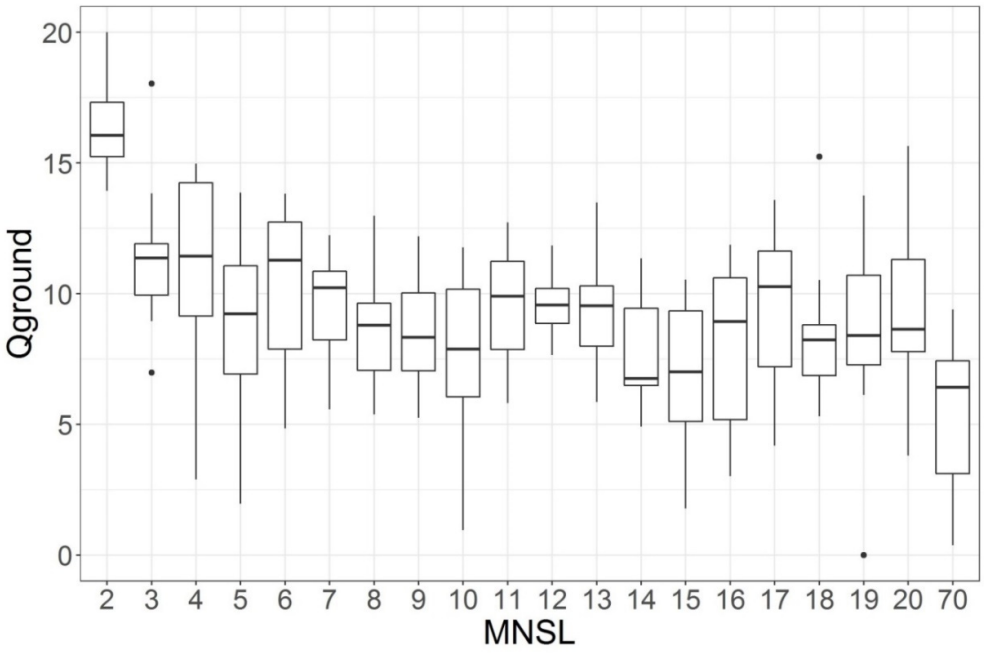

Figure S19. Ground heat flux against the MNSL at GMON W station.

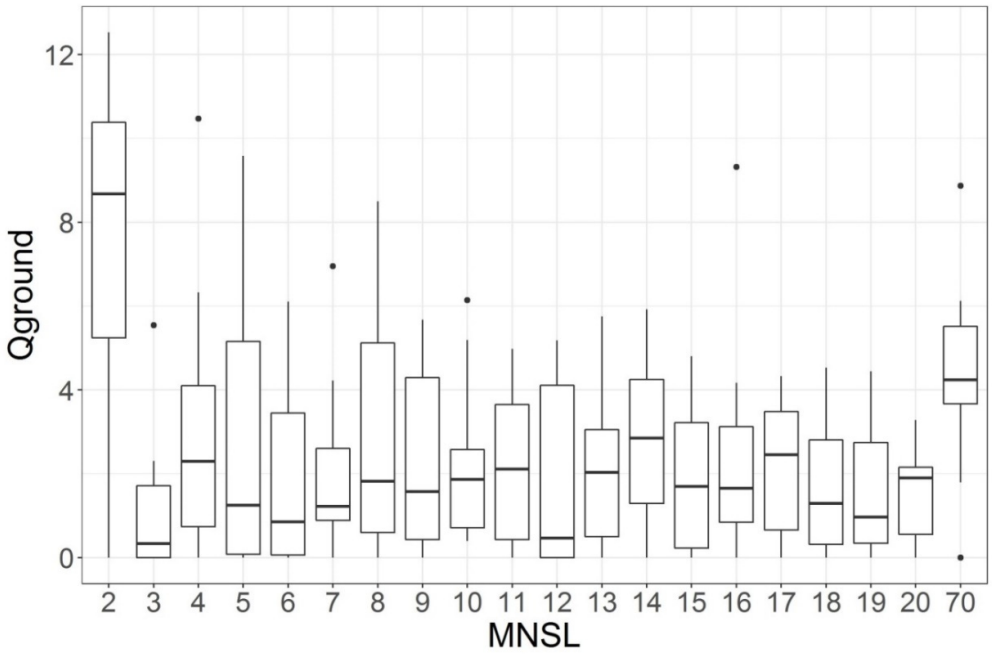

Figure S20. Ground heat flux against the MNSL at GMON Neco station.

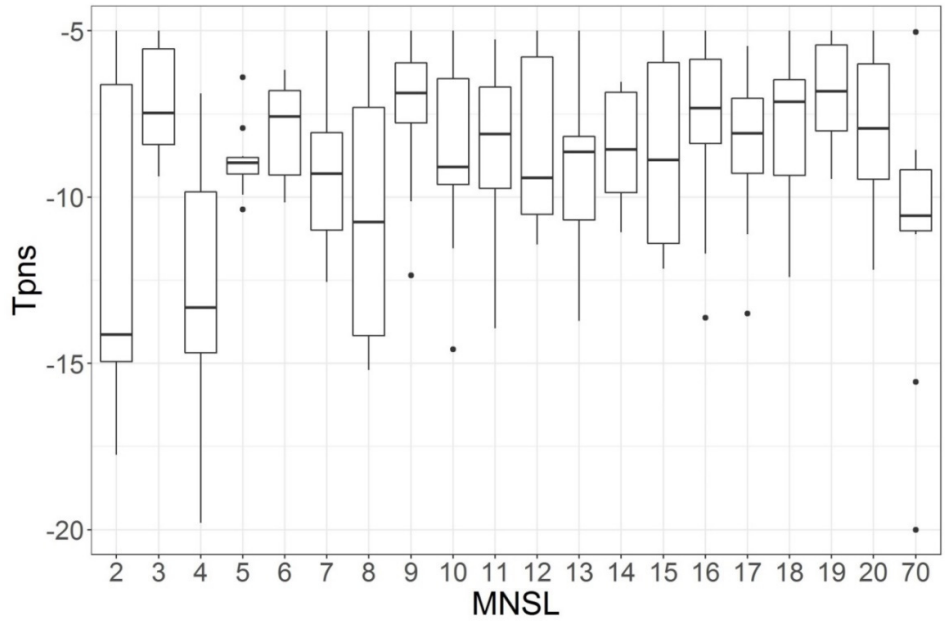

Figure S21. Atmospheric temperature threshold associated to the fresh snow minimum density against the MNSL at GMON LF station.

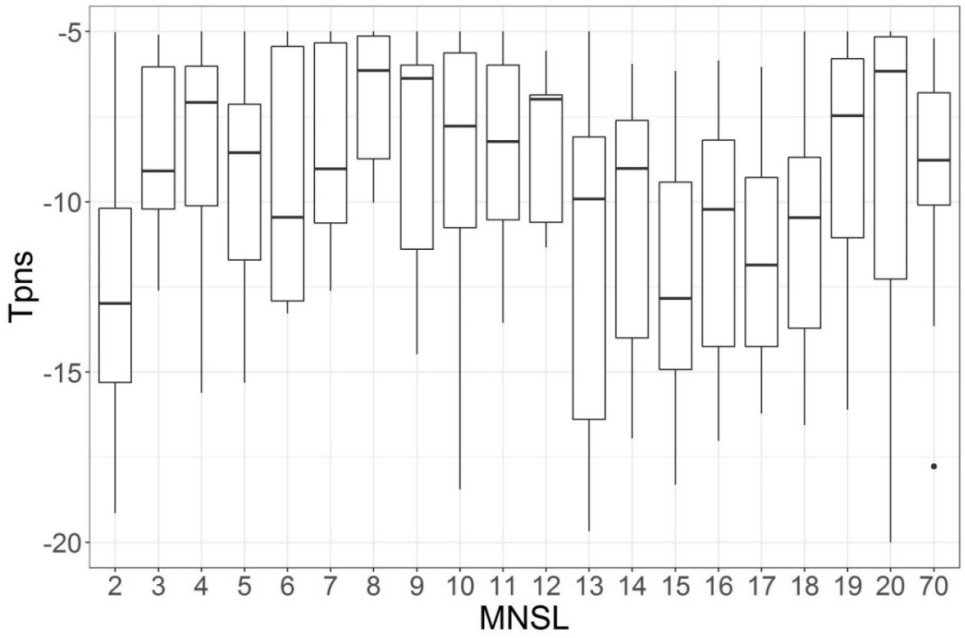

Figure S22. Atmospheric temperature threshold associated to the fresh snow minimum density against the MNSL at GMON LL station.

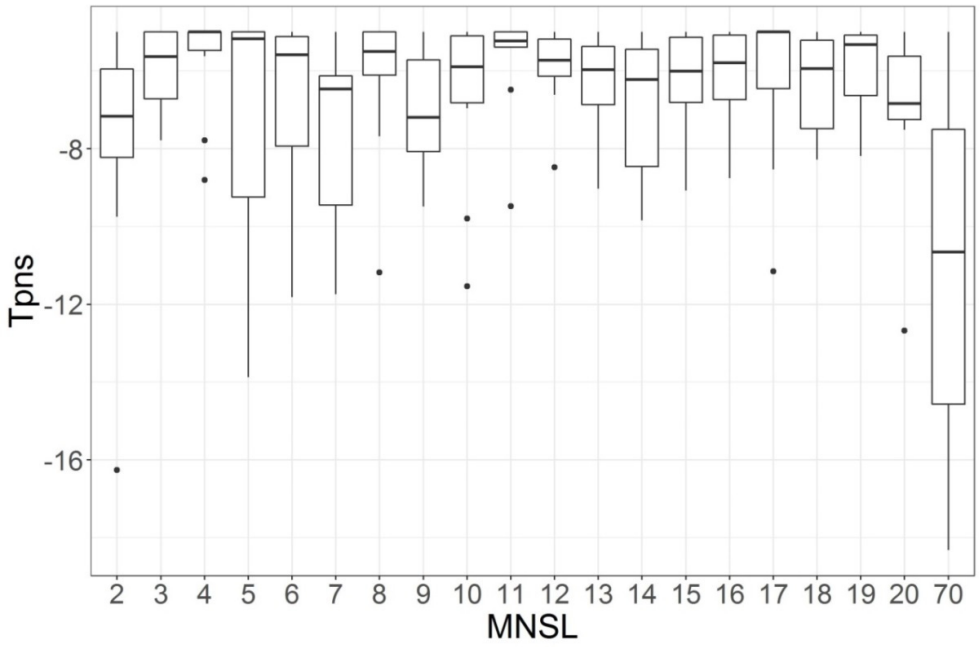

Figure S23. Atmospheric temperature threshold associated to the fresh snow minimum density against the MNSL at GMON W station.

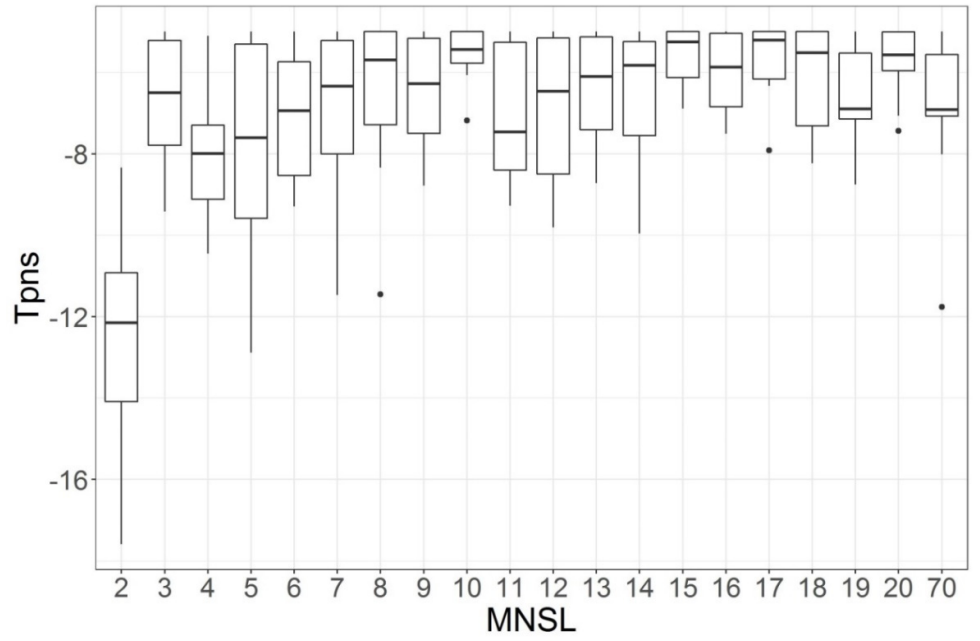

Figure S24. Atmospheric temperature threshold associated to the fresh snow minimum density against the MNSL at GMON Neco station.

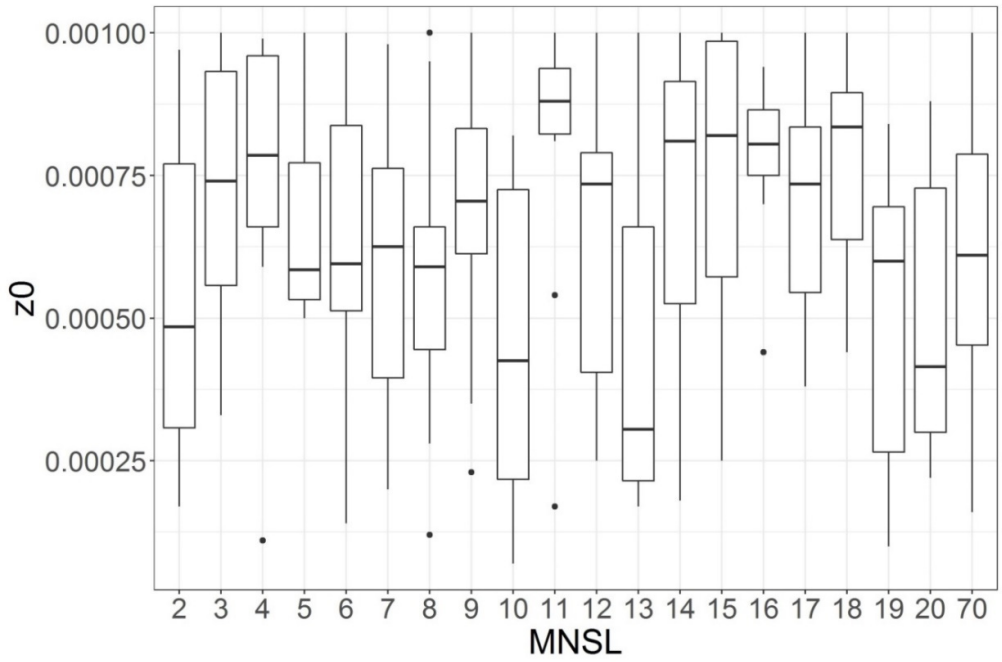

Figure S25. Snow cover surface roughness against the MNSL at GMON LF station.

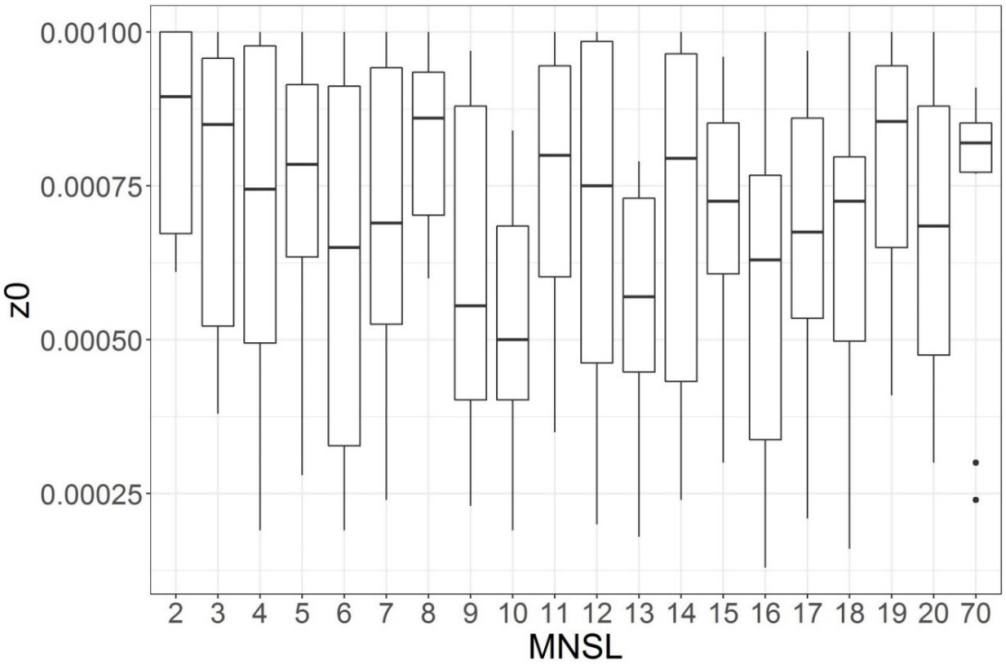

Figure S26. Snow cover surface roughness against the MNSL at GMON LL station.

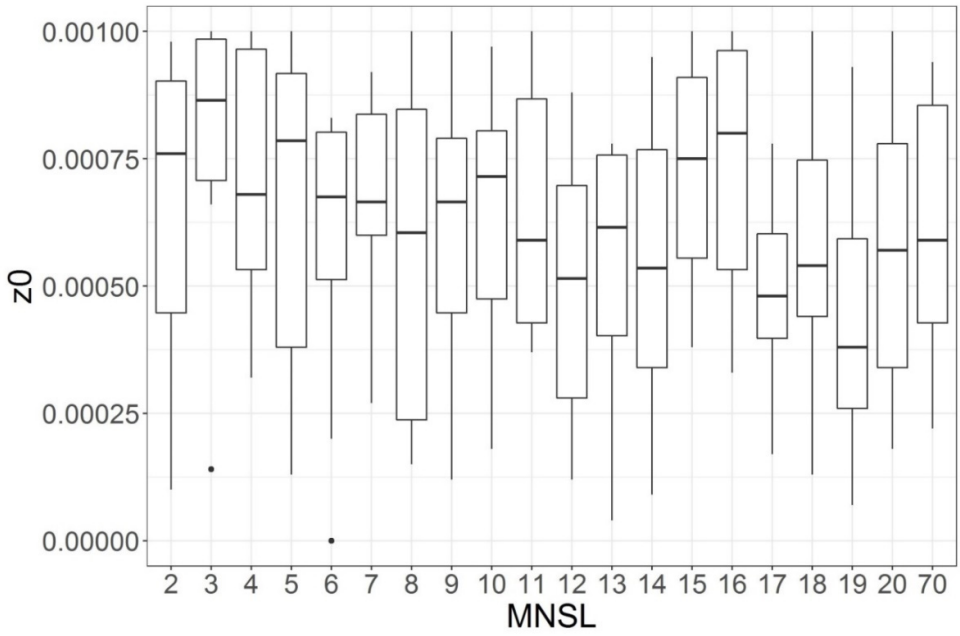

Figure S27. Snow cover surface roughness against the MNSL at GMON W station.

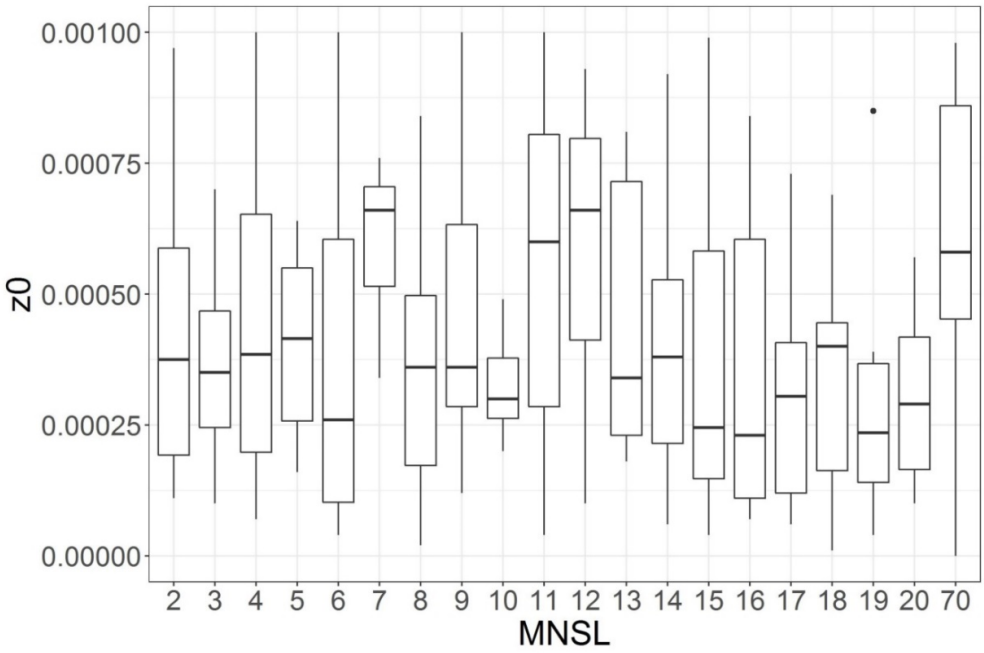

Figure S28. Snow cover surface roughness against the MNSL at GMON Neco station.

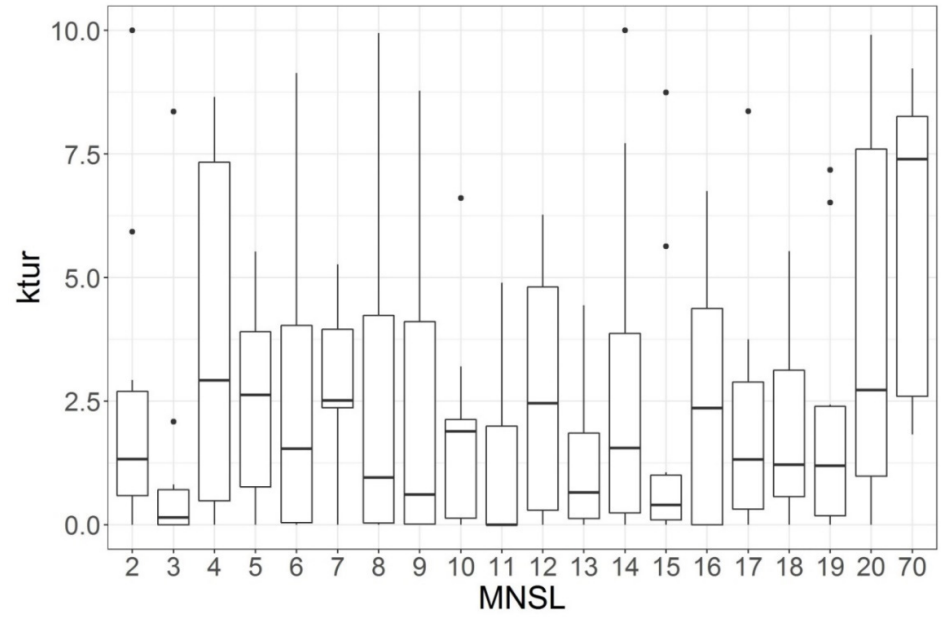

Figure S29. Reduction coefficient of the turbulent trade against the MNSL at GMON LF station.

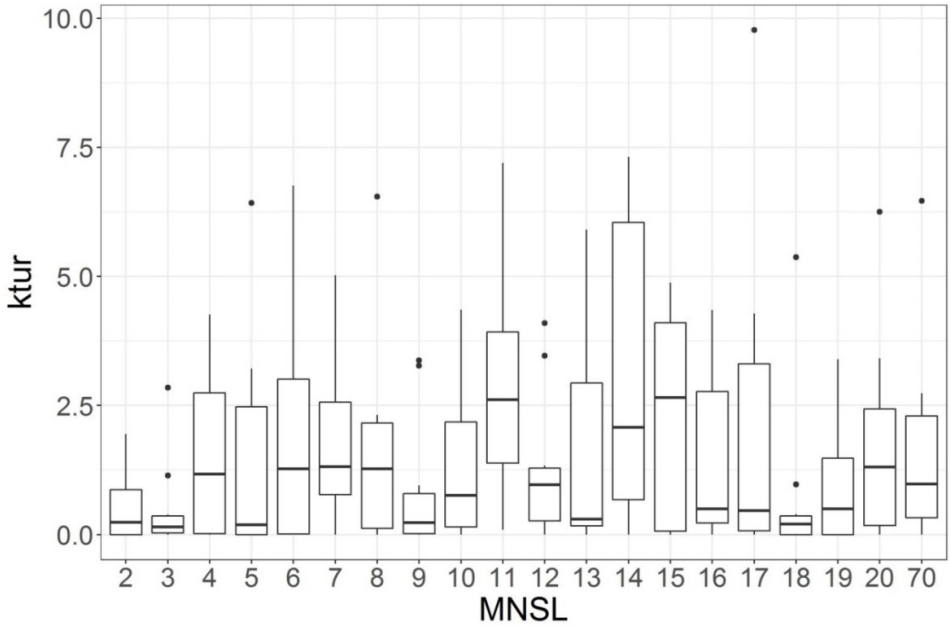

Figure S30. Reduction coefficient of the turbulent trade against the MNSL at GMON LL station.

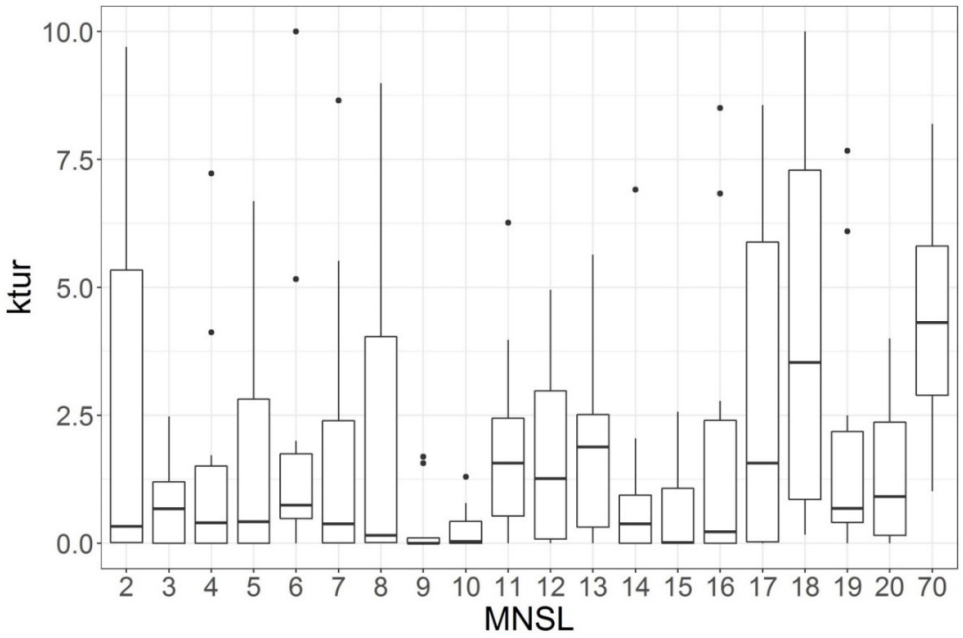

Figure S31. Reduction coefficient of the turbulent trade against the MNSL at GMON W station.

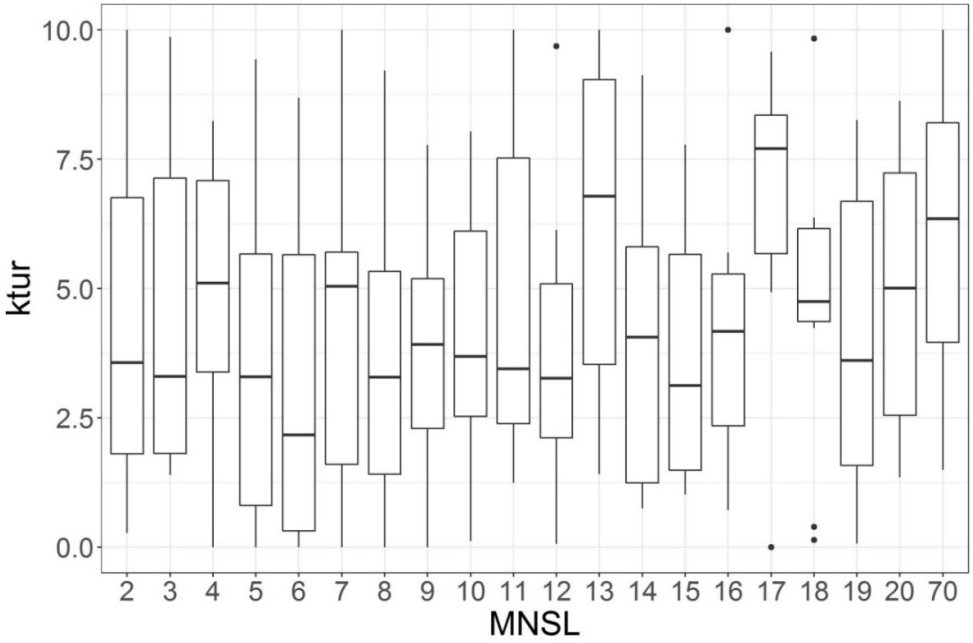

Figure S32. Reduction coefficient of the turbulent trade against the MNSL at GMON Neco station.

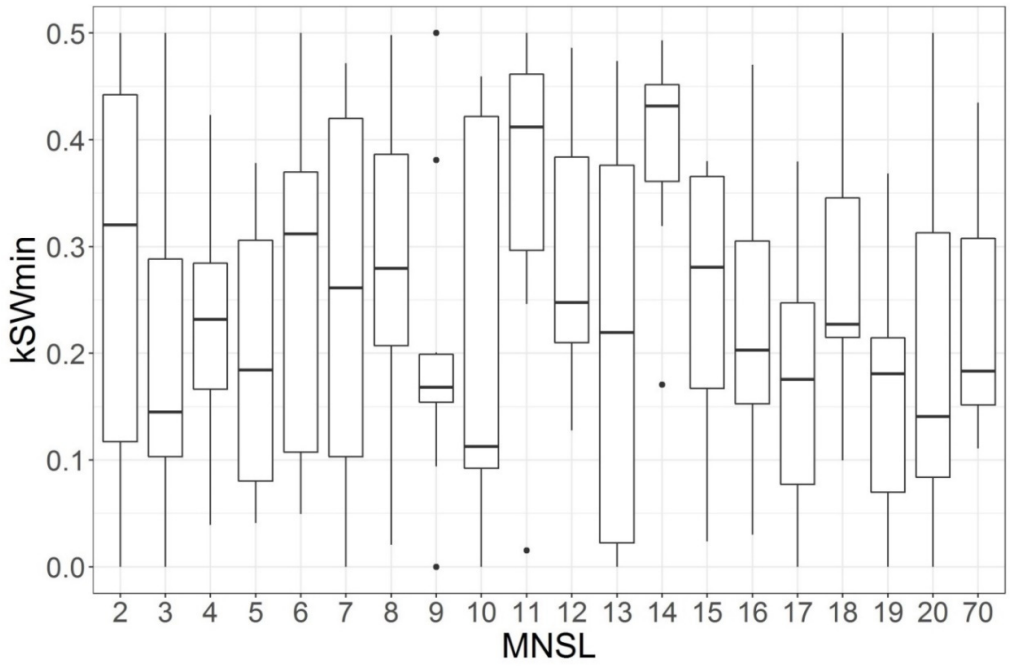

Figure S33. Minimum radiation coefficient against the MNSL at GMON LF station.

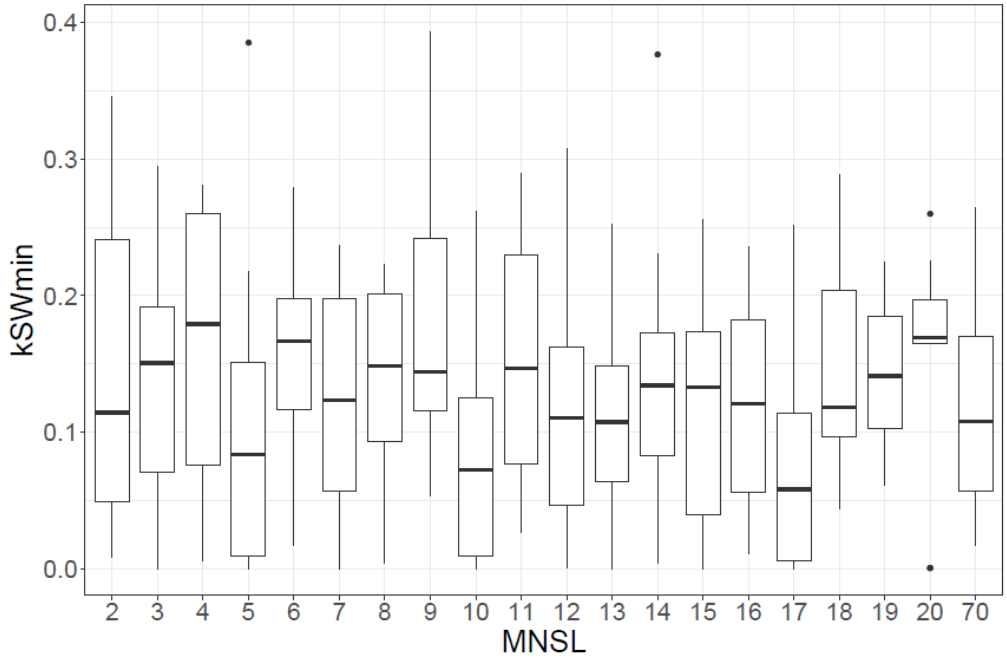

Figure S34. Minimum radiation coefficient against the MNSL at GMON LL station.

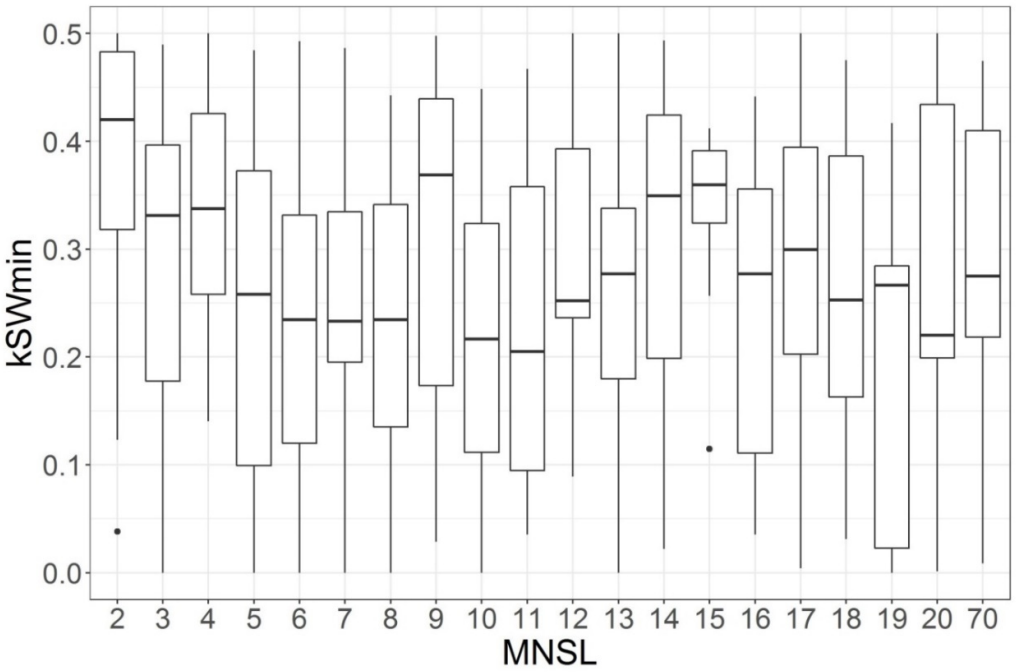

Figure S35. Minimum radiation coefficient against the MNSL at GMON W station.

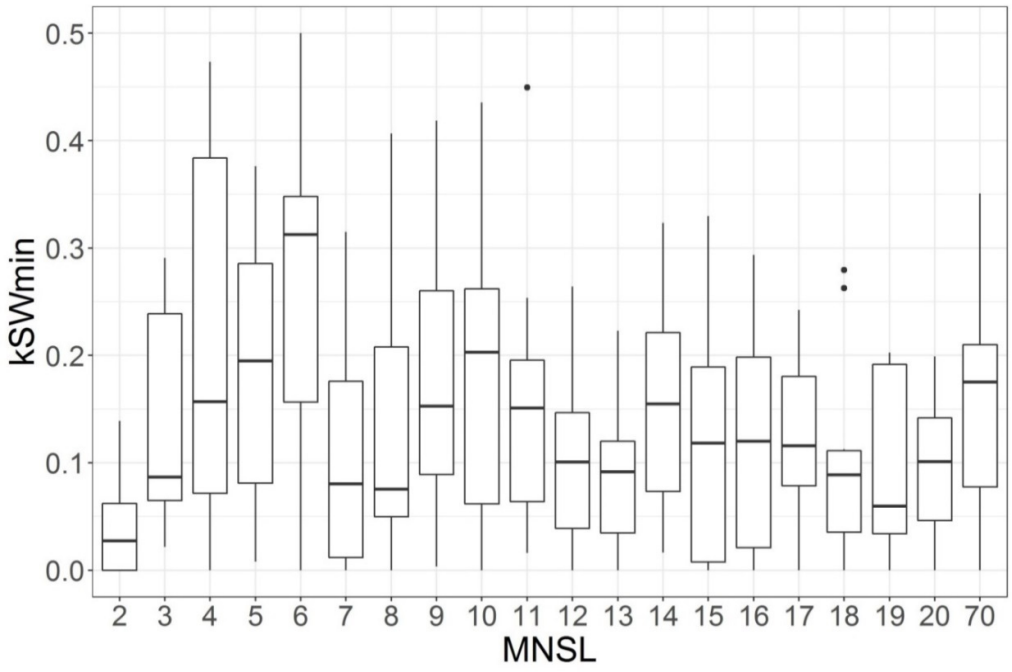

Figure S36. Minimum radiation coefficient against the MNSL at GMON Neco station.

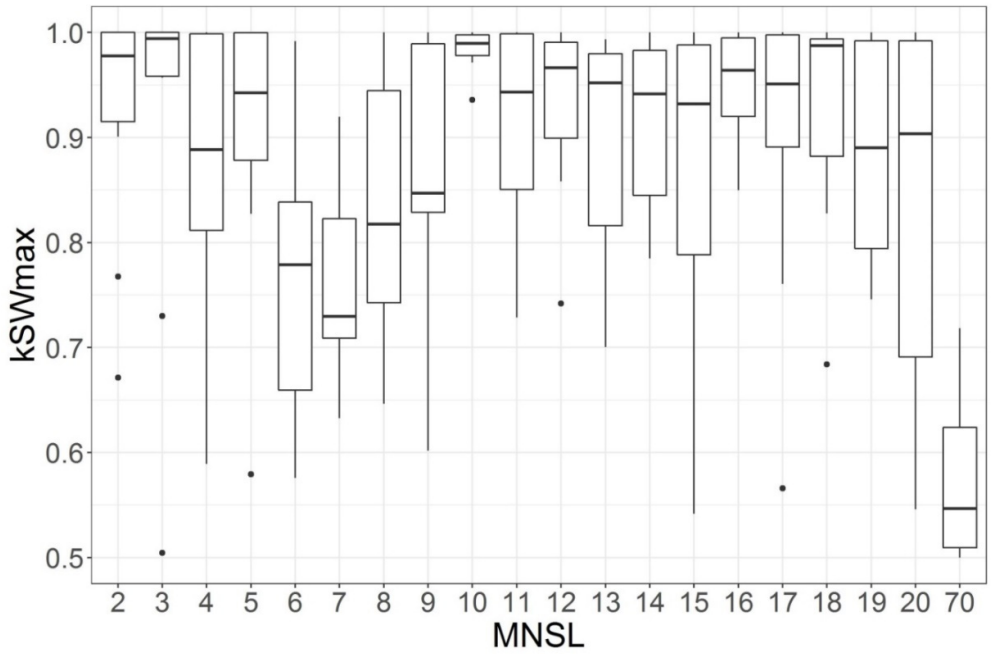

Figure S37. Maximum radiation coefficient against the MNSL at GMON LF station.

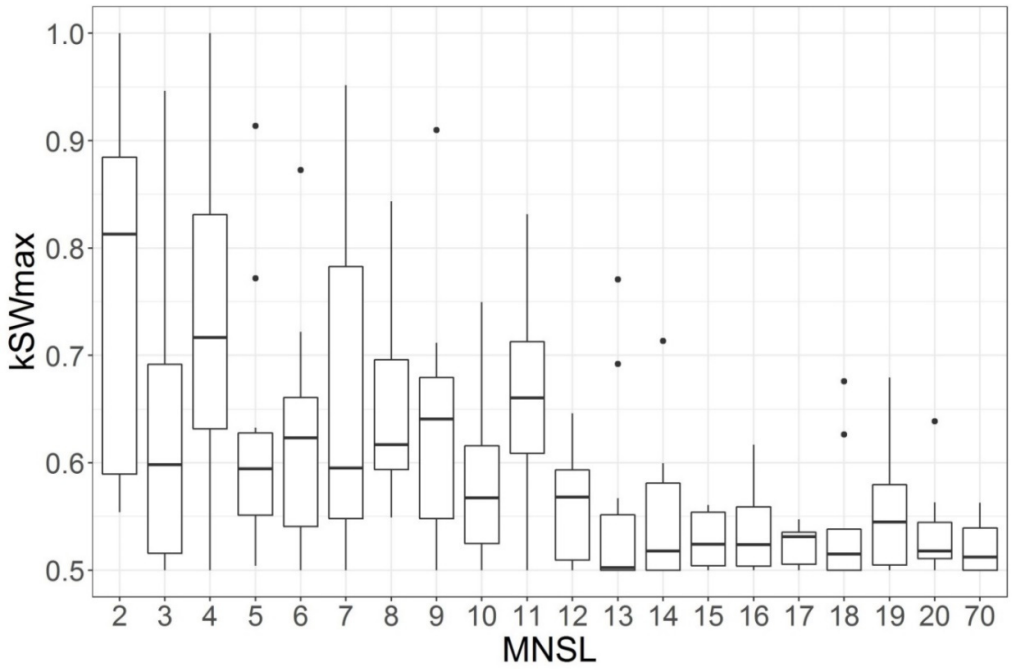

Figure S38. Maximum radiation coefficient against the MNSL at GMON LL station.

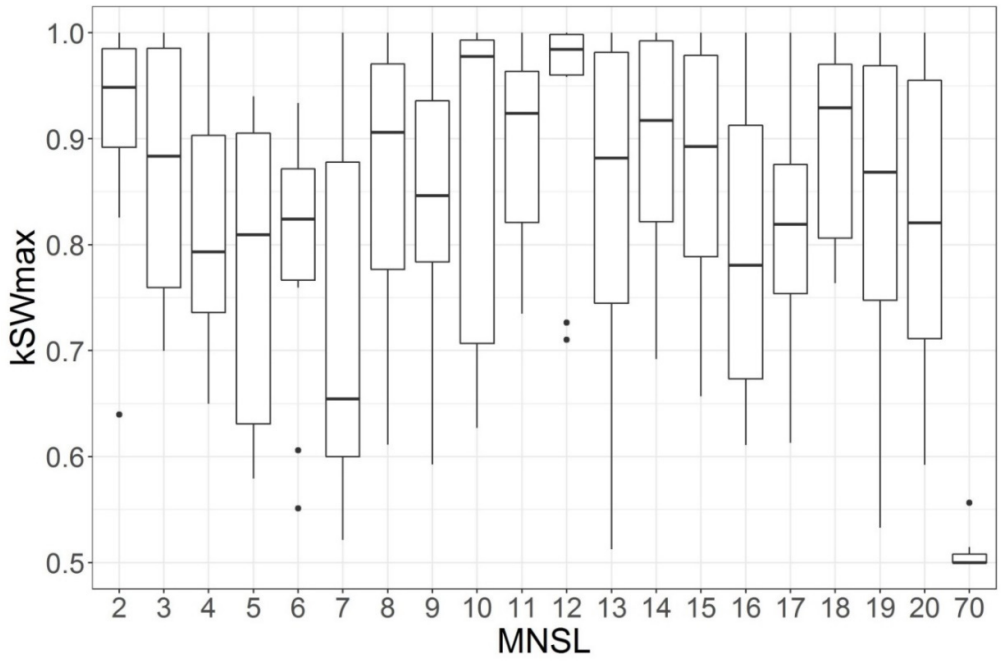

Figure S39. Maximum radiation coefficient against the MNSL at GMON W station.

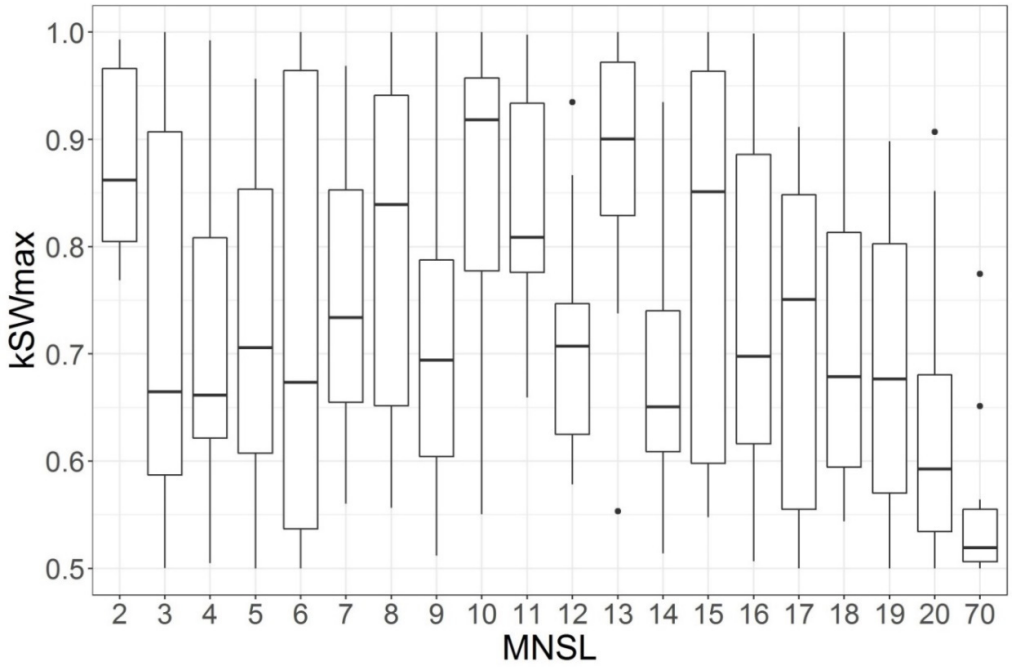

Figure S40. Maximum radiation coefficient against the MNSL at GMON Neco station.

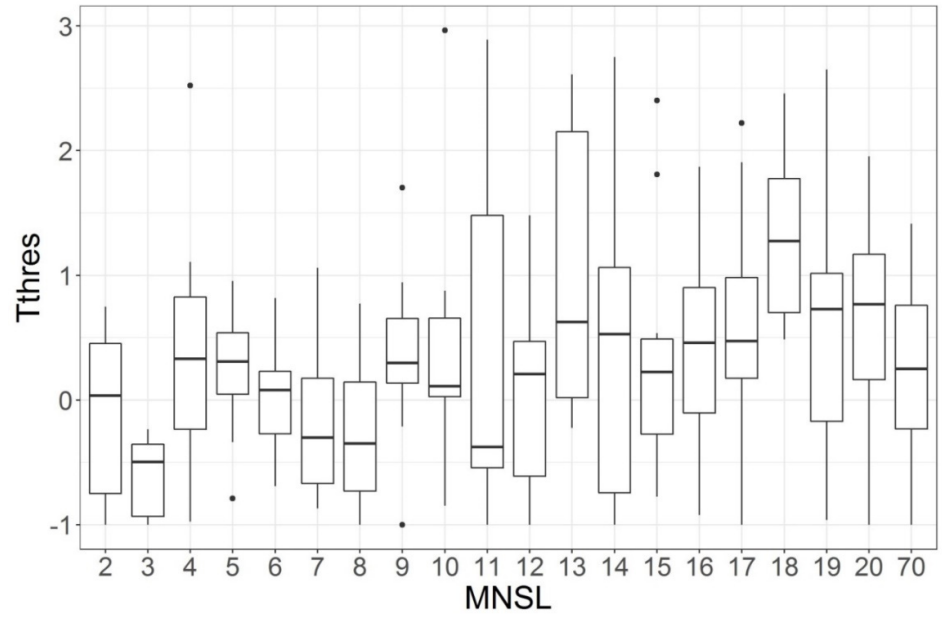

Figure S41. Threshold temperature of precipitation separation against the MNSL at GMON LF station.

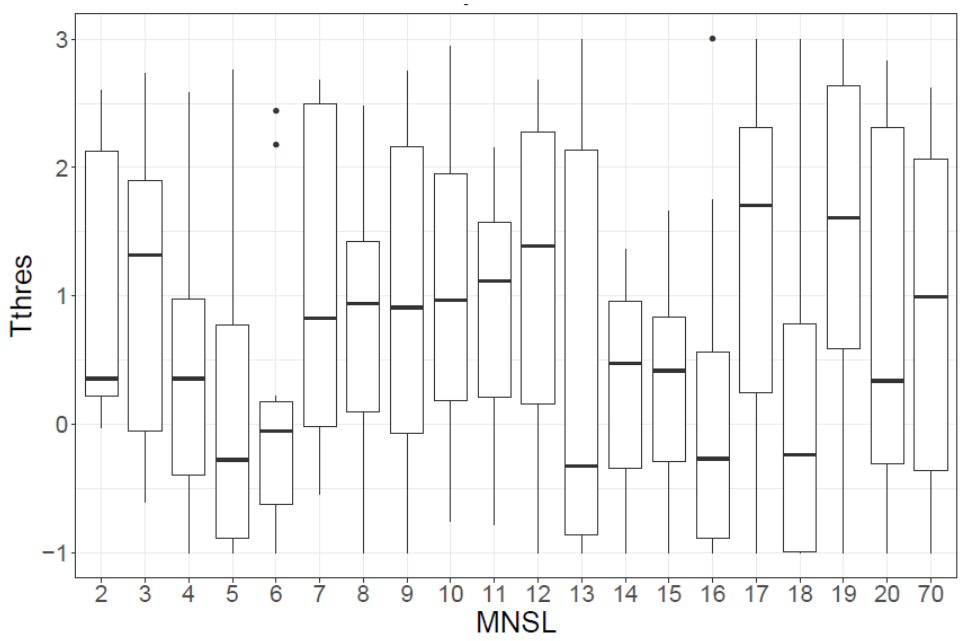

Figure S42. Threshold temperature of precipitation separation against the MNSL at GMON LL station.

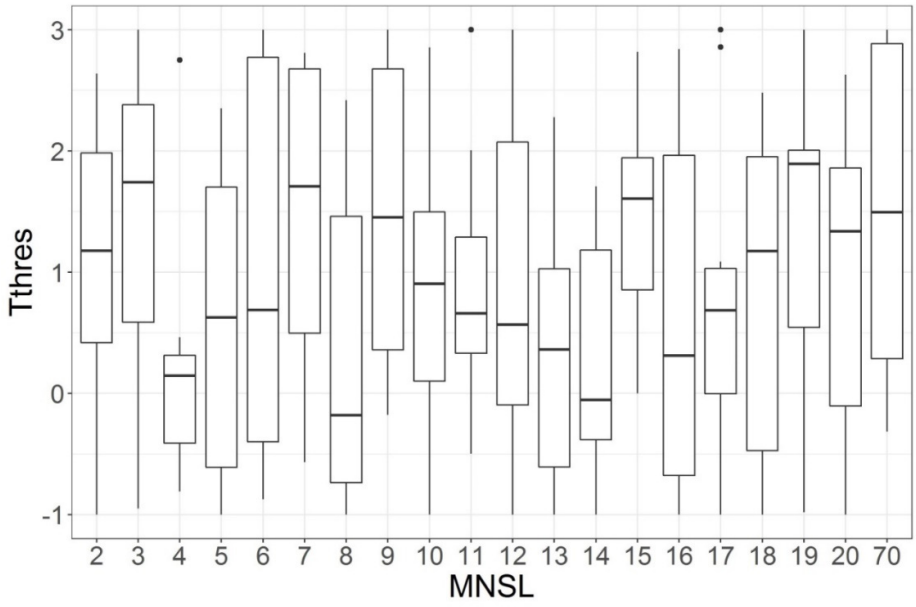

Figure S43. Threshold temperature of precipitation separation against the MNSL at GMON W station.

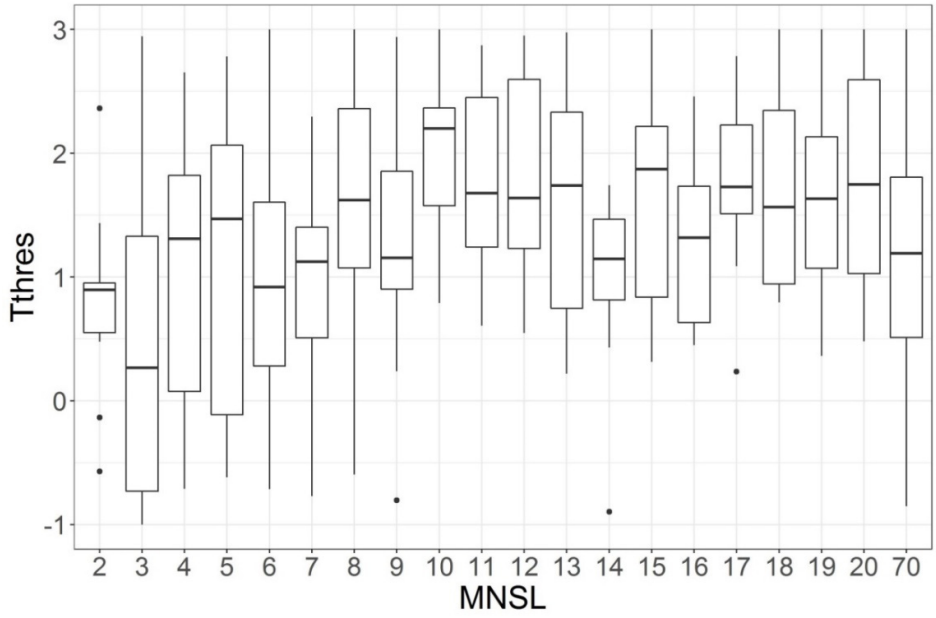

Figure S44. Threshold temperature of precipitation separation against the MNSL at GMON Neco station.